Simulation of Proton Transfer Reaction Rates: The Role of Solvent Electronic Polarization

R. I. Cukier* and Jianjun Zhu

Department of Chemistry, Michigan State University, East Lansing, Michigan 48824-1322

Received: March 25, 1997; In Final Form: June 27, 1997[⊗]

A simulation method suitable for the prediction of the rate of a proton transfer reaction of the form A--H−B → A^-−H--B^+, where -- denotes a hydrogen bond, is presented. The method is based on a golden rule formulation, where the coupling between the two proton states is obtained by solution of Schrödinger's equation for the proton states in a double-well potential whose shape is determined, in part, by the solvent's electronic polarization. The reaction activation energy is determined by solvent fluctuations, as well as flanking group (A and B) vibrational motion. The surfaces for the AB vibrational motion with the proton in its initial and final states are also modified by the coupling to the solvent's electronic polarization. Consequently, the matrix elements of the proton coupling between the AB vibronic states with the proton in its initial and final state, as well as the reaction's activation energy, are dependent upon the coupling to the solvent's electronic polarization. The rate constant for proton transfer in a representative phenol−amine hydrogen-bonded solute immersed in a polar/polarizable model for dichloromethane is simulated. The rate constant can be quite large, in the ps^{-1} range, as the proton coupling can be large for smaller AB distances, and the AB vibration provides a number of channels for proton transfer.

I. Introduction

Proton tautomerization between states that can be characterized as a shift between predominantly neutral and charge transfer configurations, such as phenol−amine hydrogen-bonded complexes, denoted here generically as AHB, involves a large charge rearrangement upon proton transfer. Schematically, the tautomerization is A--H−B → A^-−H--B^+, where -- denotes a hydrogen bond. Typically, as is well appreciated, in the gas phase the neutral state will be energetically favored, while in a polar solvent the charge transfer state will be stabilized. Many experiments on phenol−amine complexes that manipulate the gas-phase stability by chemical substitution and the solvation by changing, for example, the solvent dielectric constant confirm this tautomerization.[1]

In this article, we construct a theory for the rate of such proton transfer reactions in solution whose ingredients will be obtained by molecular dynamics simulation and quantum mechanical calculations. Special emphasis will be placed on the role that the electronic polarization of the solvent plays in determining the rate of proton transfer, and we shall see that electronic polarization effects enter in all the ingredients that characterize the rate constant. In previous work, we provided a continuum and molecular approach to electronic solvation effects on proton transfer reactions.[2]

Our approach is similar in spirit to that used to characterize nonadiabatic electron transfer reactions.[3−5] In this mechanism for charge transfer, one considers the proton potential surface parametric on the state of the solvent and finds that, for certain solvent configurations, the proton potential can be symmetrized. If the AB distance, R_{AB}, is sufficiently large, a double-well potential (symmetrized by the solvent) will be found. In this configuration, the proton can tunnel through the barrier from its initial (neutral) to its final (charge transfer) localized state. If the double well is sufficiently deep and wide, the proton energies in this symmetric well will have a pattern as shown in Figure 1. Under this circumstance, the problem is reduced to a two-level system, in the sense that the higher states are too far away in energy to contribute to the transfer process. The separation between these two energy levels gives the coupling responsible for permitting the proton to transfer between its initial and final states. The separation of the two energy levels, the protonic coupling, that depends parametrically on the R_{AB} distance, will be denoted as twice $V_{pr}(R_{AB})$. The proton transfer mechanism then is similar to that for electron transfer, with the important difference that $V_{pr}(R_{AB})$ will have a significant dependence on R_{AB}. The profile of the proton double well is quite sensitive to the distance R_{AB}; the barrier falling rapidly as R_{AB} decreases, as has been shown by quantum chemical calculations.[6,7] This is a distinguishing feature of proton transfer reactions and, in the language of charge transfer reactions, corresponds to a violation of the Condon principle used in electron transfer theory to factor out the electronic matrix element as a constant independent of the donor to acceptor distance.[5] The distinction arises because electronic wave functions are slowly varying on the scale of bond vibration displacements, while the protonic wave functions vary on the scale of bond vibration displacements. These effects have been accounted for in various theoretical treatments of proton transfer

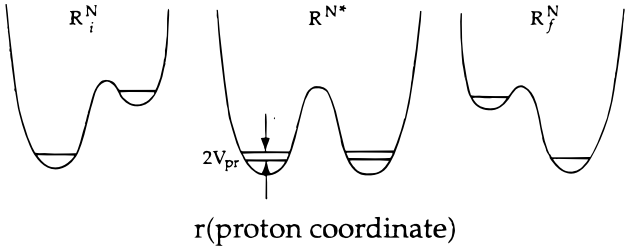

Figure 1. Proton potential surfaces (schematic) parametric on the solvent configuration, R^N. The proton surface denoted by R_i^N (R_f^N) is characteristic of a solvent configuration equilibrated to the proton's initial (final) state. The center one, with solvent configuration denoted by R^{N*}, corresponds to a configuration for which the proton can transfer, as the surface has been symmetrized by a solvent fluctuation. The proton splitting $V_{pr}(R_{AB})$ is twice the energy gap between the symmetric and antisymmetric proton states. The surfaces and splitting are parametric on the heavy atom separation R_{AB}.

[⊗] Abstract published in *Advance ACS Abstracts,* August 15, 1997.

S1089-5647(97)01063-8 CCC: $14.00

reactions and are essential to a proper treatment of such reactions.[8−14]

Another key aspect of charge transfer reactions, both electron and proton, is the role of electronic solvation in determining the reaction rate. For example, in Marcus'[4,15−17] electron transfer continuum formulation, the electronic polarization plays a crucial role in determining the activation energy, as can be immediately appreciated from the continuum dielectric expression for solvent reorganization energy. This energy is defined as the solvation energy for the process corresponding to placing the electron on the acceptor, evaluating its energy of interaction with the solvent nuclear configuration frozen at the equilibrium configuration appropriate to the initial electron state, and then letting the solvent nuclei equilibrate to this new charge distribution. This energy is proportional to $(1/\epsilon_\infty - 1/\epsilon_0)$, where ϵ_∞ is the optical and ϵ_0 is the low-frequency dielectric constant of the solvent. That the reorganization energy involves ϵ_∞ implies that, in the Franck−Condon transition of placing the electron onto the acceptor with the solvent nuclear configuration held fixed, the electronic polarization of the solvent instantaneously adjusts to the change of charge distribution. This feature follows from the much greater excitation energies of the solvent's electrons relative to that of the transferring electron. For proton transfers, a similar argument can be made, and, as the proton is typically a slower object than an electron, the time scale separation between the solvent's electronic polarization and the proton's time scale is even more dramatic. Therefore, if we want to find the proton's potential surface that will permit evaluation of its energy levels and, in this fashion, obtain the coupling $V_{pr}(R_{AB})$ responsible for the proton transfer, then we must allow for the instantaneous electronic solvation of the proton's surface. We shall refer to the proton potential surface solvated by the electronic polarization of the solvent as a *pels* (proton electronically solvated) surface. That electronic solvation can strongly influence proton transfer rates can be appreciated from the following two points. First, electronic solvation effects can be quite large. For example, the Born solvation energy (equilibrium solvation from both electronic and nuclear orientational degrees of freedom) of a charge is proportional to $(1 - 1/\epsilon_0)$, while the electronic solvation is proportional to $(1/\epsilon_\infty - 1/\epsilon_0)$. For polar solvents, the high ϵ_∞ and low ϵ_0 frequency dielectric constants satisfy $\epsilon_0 \gg \epsilon_\infty$; therefore, electronic solvation is approximately half of Born solvation energy, and this can be a large quantity. Second, the energy-level separation in the proton well is very sensitive to the barrier height. For example, WKB arguments[5] show this separation is exponentially dependent on the barrier height. Thus, electronic solvation can strongly modify the coupling, $V_{pr}(R_{AB})$.

There are a number of possible approaches to obtaining the pels surface. The one adopted here relies on molecular dynamics simulation methodology. To do so requires, then, a polar/polarizable model for the solvent. Within the context of electron transfer reactions, such models have been used previously to obtain the activation energy for the reaction that properly incorporates the distinct roles of electronic and nuclear solvent degrees of freedom.[18−21] We use a representation that has Drude dipoles centered on certain sites in the solvent molecule, the sites being characterized by scalar polarizabilities.[22−24] For this Drude model, one may solve for the induced dipoles on all the molecules for a given solvent configuration and, in this fashion, include the solvent's electronic polarizability. With such a model, we may consider a solvent nuclear configuration, and evaluate the proton's potential surface by solving for the interaction between the induced dipoles and the charge distribution of the solute that characterizes the proton's position. The polarization energy is evaluated at each proton position, and this builds up the pels surface. As the typical effect of electronic solvation is to solvate a charge distribution, the pels surface tends to be deeper than a gas-phase surface.[2] The implication is that the energy levels corresponding to the proton tunneling between the two sides of the double well tend to be closer together (smaller $V_{pr}(R_{AB})$ values); tunneling is suppressed, relative to what would be predicted in the absence of the electronic solvation.

There is another important role for electronic solvation that must be incorporated in the proton transfer rate constant. As noted above, the R_{AB} distance is modulated by the AB vibration, and the rate constant will involve matrix elements of the coupling $V_{pr}(R_{AB})$ with the vibronic eigenfunctions in the R_{AB} potential surfaces for the initial and final proton states.[8−14] These surfaces in the R_{AB} vibrational coordinate are not simply the gas-phase ones but are also solvated by the electronic polarization of the solvent. Because the AB vibrational period is much longer than the electronic time scale, we may, as for the proton coordinate, adiabatically (in the Born−Oppenheimer (BO) sense) solvate these R_{AB} surfaces. When the proton is in its initial, neutral state, this solvation is not very dependent on R_{AB}, but, for the charge transfer state, increasing R_{AB} (separating charge) leads to a large increase in the electronic solvation. Thus, especially for the final proton state, the electronically solvated R_{AB} surface is quite different than would be predicted from the gas-phase surface. It should also be pointed out that typical AB bond vibration frequencies for these phenol−amine complexes are around 250 cm^{-1}; therefore, the bond vibrations should be treated quantum mechanically and we shall do so in this work. Furthermore, we shall see that a harmonic model for the R_{AB} vibration is not very accurate for the purposes of obtaining the proton transfer rate constant.

There are now quite a few theoretical and computational approaches to the prediction of proton transfer rates. Many theoretical and simulation approaches have focused on the reduced two-level system, nonadiabatic regime,[10,11,13,25,26] although stronger coupling has also been considered.[14,25,27] The importance of the R_{AB} vibration was recognized early on[8,9] and has been an integral part of recent theories[10−14] and simulations.[26] Aspects of stronger hydrogen bonding, where the two-level approach is not applicable, have been studied by various classical/quantum simulation methods.[28−39] Path integral methods, which can span the coupling from the nonadiabatic to the adiabatic regime,[40,41] have been used and have included solvent electronic polarization.[42] Borgis and Hynes[14] presented a theory of proton transfer that spans the nonadiabatic and adiabatic regimes with the use of Landau−Zener type of theory and incorporated the effect of the R_{AB} vibration on the rate constant. We develop similar formal expressions but do so for the electronically solvated proton and R_{AB} surfaces. With the formal expression in hand, we then use molecular dynamic simulation and quantum mechanical methods to obtain all the parameters that enter the rate expression.

The plan of the remainder of this paper is as follows. In section II, we present the formalism that introduces an expression for the proton transfer rate constant in terms of the various ingredients required for its evaluation. Then, we discuss how molecular dynamics and quantum mechanics can be used to obtain these quantities. In section III, these quantities are evaluated for a representative model of the hydrogen-bonded complex and for a polar/polarizable solvent model of dichloromethane. The rate constant is evaluated in section IV, and we present concluding remarks in section V.

II. Rate Constant Formalism

In this section, we will obtain an expression for the proton transfer rate constant. Our procedure will be based on the separation of time scales:

$$\tau_{\rm el} < \tau_{\rm pr} < \tau_{R_{\rm AB}} < \tau_{R^{\rm N}}$$

where the times $\tau_{\rm el}$, $\tau_{\rm pr}$, $\tau_{R_{\rm AB}}$, and $\tau_{R^{\rm N}}$ denote, respectively, the time scales for the electronic fluctuations of the solvent, the proton transfer, the $R_{\rm AB}$ vibration, and the dominant modes of the solvent (as found from, for example, the dielectric spectrum). The first inequality corresponds, in Marcus' continuum dielectric approach,[43] to the solvent's electronic polarization being faster than all the other time scales, and it is even more appropriate than for electron transfer reactions, as proton excitation energies are smaller than those of transferring electrons. The heavy-atom vibration, which we shall treat quantum mechanically, is viewed as a slower motion than the proton's transfer time scale. Thus, qualitatively, the proton transfers parametrically on the heavy-atom separation, as appropriate to their difference in masses. Finally, we shall assume that the solvent nuclear motion is characterized microscopically by fluctuations that correspond to the orientational polarization in dielectric parlance. These are indeed mainly of lower frequency than the typical flanking-heavy-atom vibration frequencies in hydrogen bonds.[5] Using this separation of time scales, we may formulate a hierarchy of Born−Oppenheimer equations, as we now describe, and then use them to obtain the proton transfer rate constant.

The Hamiltonian for the solute, the solvent, and their interactions may be written as

$$H = T_{\rm r} + T_{R_{\rm AB}} + T_{R^{\rm N}} + V_{\rm pels}(r,R_{\rm AB}|R^{\rm N}) \qquad (2.1)$$

where

$$V_{\rm pels}(r,R_{\rm AB}|R^{\rm N}) = V_{\rm g}(r,R_{\rm AB}) + V_{\rm els}(r,R_{\rm AB}|R^{\rm N}) + V_{\rm in}(r,R_{\rm AB}|R^{\rm N}) + V_{\rm solv}(R^{\rm N}) \qquad (2.2)$$

In eq 2.2, $V_{\rm g}(r,R_{\rm AB})$ is the gas-phase potential energy surface for the proton coordinate r, as measured from the A atom, and $R_{\rm AB}$ is the heavy-atom relative coordinate. The terms $V_{\rm in}$ and $V_{\rm solv}$ represent the solute−solvent and solvent−solvent permanent charge and van der Waals interactions. The potential energy $V_{\rm els}$ incorporates the effect that the solvent electronic degrees of freedom have on the solute, parametric on the proton's and the heavy atoms' relative coordinate. The potential $V_{\rm els}$ also depends on the solvent nuclear configuration, denoted by $R^{\rm N}$. As the electronic degrees of freedom are much faster than those of the proton and heavy-atom vibration (and the solvent nuclear degrees of freedom), they adjust instantaneously to changes in these coordinates; this electronic solvation is equilibrium solvation. Instead of introducing an explicit Hamiltonian for these electronic degrees of freedom, we may obtain this contribution to the solvation energy from the expression[44]

$$V_{\rm els}(r,R_{\rm AB}|R^{\rm N}) = -\frac{1}{2}\sum_i \mathbf{p}_i\cdot\mathbf{E}_i^0 \qquad (2.3)$$

The induced dipoles of the solvent $\mathbf{p}_i$ are obtained according to the scheme[19−24]

$$\mathbf{p}_i = \alpha_i[\mathbf{E}_i^0 + \sum_{j\neq i}\mathbf{T}_{ij}\cdot\mathbf{p}_j] \qquad (2.4)$$

with

$$\mathbf{E}_i^0 = \sum q_j\frac{\hat{\mathbf{r}}_{ij}}{r_{ij}^2} \quad \mathbf{T}_{ij} = \frac{1}{r_{ij}^3}[3\hat{\mathbf{r}}_{ij}\hat{\mathbf{r}}_{ij} - 1] \qquad (2.5)$$

In these equations, α_i is the polarizability of the ith molecular site, the q_i's denote the charges assigned to sites in the molecules to represent the electrostatic part of the intermolecular interactions, and the $\mathbf{T}_{ij}$ tensor characterizes the induced dipole interactions for sites separated by vectors $\mathbf{r}_{ij}$. The field $\mathbf{E}_i^0$ on the ith site in a particular solvent molecule arises from the charge sites in the other molecules as well as the charge sites in the solute. Thus, this field is parametric on the proton and heavy-atom positions. For reactions involving charge transfer, this representation is natural, as it mimics the electronic polarization of continuum electrostatics that instantaneously equilibrates to the solute charge distribution. Of course, this electronic solvation energy is for a particular solvent nuclear configuration, as we have indicated with the parametric notation $R^{\rm N}$, in eqs 2.1 and following. Now consider the Hamiltonians H_i and H_f obtained by localizing the proton at its initial (i) or final (f) position. We shall take, as these initial and final states, the neutral and charge transfer configurations of the proton, respectively. These Hamiltonians are

$$H_i = T_{R_{\rm AB}} + T_{R^{\rm N}} + V_{\rm pels}^i(R_{\rm AB}|R^{\rm N})$$

$$H_f = T_{R_{\rm AB}} + T_{R^{\rm N}} + V_{\rm pels}^f(R_{\rm AB}|R^{\rm N}) \qquad (2.6)$$

where

$$V_{\rm pels}^i(R_{\rm AB}|R^{\rm N}) \equiv V_{\rm pels}(r{=}r_i,R_{\rm AB}|R^{\rm N}) \qquad (2.7)$$

and a corresponding definition holds for the final proton state. If we carry out a molecular dynamics simulation that constructs these energies for the i and f state charge distributions of the solute, there will be configurations where these energies are essentially equal. Once we find these solvent configurations, denoted by $R^{\rm N*}$, they will be appropriate configurations, in principle, for the proton to transfer. Therefore, for these solvent configurations, we will construct, for fixed $R_{\rm AB}$ values, the proton potential energy surface $V_{\rm pels}(r,R_{\rm AB}|R^{\rm N*})$ by carrying out the same electronic solvation simulation as described above, but now parametric on the proton's position, for a given $R^{\rm N*}$ value. This surface should approximate a double-well symmetric potential. We may solve the Schrödinger equation

$$[T_{\rm r} + V_{\rm pels}(r,R_{\rm AB}|R^{\rm N*})]\psi_p(r,R_{\rm AB}|R^{\rm N*}) = \epsilon_p(R_{\rm AB}|R^{\rm N*})\psi_p(r,R_{\rm AB}|R^{\rm N*}) \qquad (2.8)$$

for the wave functions $\psi_p(r,R_{\rm AB}|R^{\rm N*})$ and energies $\epsilon_p(R_{\rm AB}|R^{\rm N*})$ of the proton in this potential. If the two lowest energy states ($p = 1$ and 2), denoted henceforth as ϵ_+ and ϵ_-, respectively, which are the symmetric and antisymmetric (delocalized) eigenstates in this double-well potential, are well separated from the higher lying states, then we may consider a two-level system approach to obtaining the proton transfer rate constant. And, we may use their separation to provide the coupling that is responsible for the proton transfer. Of course, the symmetric double wells for different solvent configuration $R^{\rm N*}$ will provide different eigenvalues, and not all of them may satisfy our requirement of a two-level system. But, as long as this is the case on the average, then we may proceed with a two-level system approach. Thus, we shall use the average value (over $R^{\rm N*}$ configurations) of this separation to provide the coupling

$V_{pr}(R_{AB})$ responsible for the proton transfer:

$$V_{pr}(R_{AB}) = \langle(\epsilon_- - \epsilon_+)(R^{N*})/2\rangle_{R^{N*}} \quad (2.9)$$

(The factor of 2 in the definition of $V_{pr}(R_{AB})$ reflects the connection between the diabatic, localized state approach to constructing the rate constant for charge transfer, and the adiabatic delocalized states that result from solving for eigenstates in the proton potential energy surface.)[45] The averaged (over the solvent configurations that have symmetrized the proton potential energy surface) protonic coupling $V_{pr}(R_{AB})$ is parametrically dependent on the heavy-atom separation. And, it is this significant dependence on R_{AB} that lends much of the distinctive character to a proton transfer reaction formalism relative to that required for electron transfer. In this fashion, we may construct the coupling responsible for the proton transfer.

Another ingredient required for the formulation of the rate constant is the characterization of the heavy-atom vibration by the wave functions and energies that its potential surface supports. To construct these quantities, consider the solution of the Schrödinger equation in the BO scheme where we now want to separate the heavy-atom R_{AB} and solvent R^N motion. Because the R_{AB} motion is a vibration on the $\sim$250 cm^{-1} frequency scale[1] and the important solvent fluctuations are described by orientational and similar low-frequency motions, this is a natural separation scheme. It permits a fully quantum mechanical treatment of the vibration that is warranted, as this frequency is greater than k_BT. Thus, using the definition in eq 2.7, we construct a BO scheme from

$$[T_{R_{AB}} + V^i_{pels}(R_{AB}|R^N)]\phi^i_{n_i}(R_{AB}|R^N) = E^i_{n_i}(R^N)\phi^i_{n_i}(R_{AB}|R^N) \quad (2.10)$$

and the analogous equation for the *f* state. The eigenfunctions and energies are dependent on the solvent nuclear configuration R^N. Once again, it is a useful approximation scheme to construct these quantities from the averaged surface. Thus, we shall actually construct $\phi^i_{n_i}(R_{AB})$ and $E^i_{n_i}$ from the configuration-averaged surface $V^i_{pels}(R_{AB})$, and similarly for the final state. These surfaces are quite distinct from the corresponding gas-phase surfaces, as the electronic solvation energy increases as the R_{AB} distance is increased. This will be especially true for the *f* state, as this one is the charge transfer state.

If we were to treat the solvent nuclear degrees of freedom as quantum mechanical, then the other BO equation to solve is

$$[T_{R^N} + E^i_{n_i}(R^N)]\chi^{n_i}_{m_i}(R^N) = E^{n_i}_{m_i}\chi^{n_i}_{m_i}(R^N) \quad (2.11)$$

The eigenvalues $E^{n_i}_{m_i}(R^N)$ and $E^{n_f}_{m_f}(R^N)$ are the energies of the solvent states in the nuclear solvation wells for the *i* and *f* states that in charge transfer reactions are viewed as arising mainly from the solvent orientational polarization. Theory and simulation conclude that these are well represented as harmonic surfaces, although there is no fundamental requirement for such a restriction. The index m_i refers to the vibronic states in the *i*-state solvent nuclear coordinate wells. From the perspective of simulation, this coordinate is taken as the permanent charge and van der Waals parts of the interaction energy between the solute and solvent molecules. In principle, these vibronic wave functions and energies are dependent on the state of excitation in the R_{AB} well, the n_i quantum number. But, it should be clear that heavy-atom R_{AB} wave functions are very space localized relative to the length scale of the interaction with the solvent. Therefore, we may make the replacements

$$\chi^{n_i}_{m_i}(R^N) = \chi_{m_i}(R^N,\langle R_{AB}\rangle_{n_i}) = \chi_{m_i}(R^N,R^{i,eq}) \approx \chi_{m_i}(R^N,R^{f,eq})$$
$$\approx \chi_{m_i}(R^N,R^{eq}) \equiv \chi_{m_i}(R^N) \quad (2.12)$$

where R^{eq} denotes the common value of $R^{i,eq}$ and $R^{f,eq}$. The last approximation arises from the small displacement of the R_{AB} equilibrium position between the *i* and *f* surfaces (*vide infra*).

With the above ingredients, we may now formulate the rate constant for proton transfer, using the golden rule,[5] where the perturbation is $V_{pr}(R_{AB})$ and there are two modes (the R_{AB} vibration and the solvent R^N) driving the process. A convenient starting form is[5]

$$k = \sum_{n_i}\sum_{m_i}\rho_{n_i}\rho_{m_i}\sum_{n_f}\sum_{m_f}|\langle\phi^i_{n_i}(R_{AB})|V_{pr}(R_{AB})|\phi^f_{n_f}(R_{AB})\rangle|^2| \times$$
$$\langle\chi_{m_i}(R^N)|\chi_{m_f}(R^N)\rangle|^2 \times \delta(E_{m_f} - E_{m_i} + E^f_{n_f} - E^i_{n_i}) \quad (2.13)$$

Here, ρ_{m_i} and ρ_{n_i} are, respectively, the equilibrium distribution functions for the solvent R^N and heavy-atom R_{AB}, when the proton is in its initial state. The delta function accounts for energy conservation. This rate constant expression can be reduced to a more convenient form for simulation by separating the contributions of the two modes via the identity $\delta(x - y) = \int d\epsilon\ \delta(x - \epsilon)\ \delta(\epsilon - y)$.[46] Then, eq 2.13 becomes

$$k = \int d\epsilon\ G_{R_{AB}}(\epsilon)\ G_{R^N}(\epsilon)$$

where

$$G_{R_{AB}}(\epsilon) = \sum_{n_i}\rho_{n_i}\sum_{n_f}|\langle\phi^i_{n_i}(R_{AB})|V_{pr}(R_{AB})|\phi^f_{n_f}(R_{AB})\rangle|^2 \times$$
$$\delta(E^f_{n_f} - E^i_{n_i} + \epsilon)$$

and

$$G_{R^N}(\epsilon) = \sum_{m_i}\rho_{m_i}\sum|\langle\chi_{m_i}(R^N)|\chi_{m_f}(R^N)\rangle|^2\delta(E_{m_f} - E_{m_i} - \epsilon) \quad (2.14)$$

As noted above, it is sensible to treat the solvent classically, as the frequencies that couple to the charge transfer strongly are much smaller than k_BT. Using the classical nature of the solvent nuclear motion, the function $G_{R^N}(\epsilon)$ becomes[47]

$$G_{R^N}(\epsilon) = \sqrt{\frac{\pi\hbar^2}{\lambda_s k_B T}}e^{-(\lambda_s + \Delta G^0 + \epsilon)^2/4\lambda_s k_B T} \quad (2.15)$$

Combining eqs 2.14 and 2.15 produces the rate constant expression

$$k = \sum_{n_i}\rho_{n_i}\sum_{n_f}|\langle\phi^i{}_{n_i}(R_{AB})|V_{pr}(R_{AB})|\phi^f{}_{n_f}(R_{AB})\rangle|^2 \times$$
$$\sqrt{\frac{\pi\hbar^2}{\lambda_s k_B T}}e^{-(\lambda_s + \Delta G^0 + E^f_{n_f} - E^i_{n_i})^2/(4\lambda_s k_B T)}$$

$$\equiv \sum\rho_{n_i}\sum V^2_{n_i,n_f}\sqrt{\frac{\pi\hbar^2}{\lambda_s k_B T}}e^{-(\lambda_s + \Delta G^0 + E^f_{n_f} - E^i_{n_i})^2/(4\lambda_s k_B T)} \equiv$$
$$\sum_{n_i}\rho_{n_i}\sum_{n_f}k_{n_i n_f} \quad (2.16)$$

where we have defined the matrix element $V_{n_in_f}$ of the protonic coupling $V_{pr}(R_{AB})$ as

$$V_{n_in_f} = |\langle\phi^i_{n_i}(R_{AB})|V_{pr}(R_{AB})|\phi^f_{n_f}(R_{AB})\rangle| \qquad (2.17)$$

The use of a classical solvent has resulted in the solvent reorganization energy λ_s appearing in the activation energy for the reaction, and we have now made explicit the reaction free energy ΔG^0.

The last equality in eq 2.16 emphasizes that we may view the proton transfer rate constant as arising from a sum over thermally weighted initial-state channels and final-state channels corresponding to the different vibronic states in the heavy-atom vibrational well for the proton initial and final states. Each channel rate constant $k_{n_in_f}$ has its own "effective" activation energy. The difference between an electron transfer reaction rate constant with a coupling to two nuclear degrees of freedom, one treated classically and one quantum mechanically, is that here the feature that the coupling $V_{pr}(R_{AB})$ has a rapid dependence on R_{AB} prevents a Condon approximation on the R_{AB} matrix element, whereby $V_{pr}(R_{AB}) \approx V_{pr}(R^{eq}_{AB})$ would come out as a parameter and there would be Franck−Condon factors for the R_{AB} degree of freedom.

One final modification of eq 2.16 is worth carrying out. Because $V_{pr}(R_{AB})$ can become large as the R_{AB} distance decreases, the golden rule formulation can break down, even if the two-state approximation is valid. Then, the mechanism of proton transfer switches from the nonadiabatic (golden rule) regime to the adiabatic regime. Incorporating this possibility can be carried out by following a Landau−Zener[48,49] type of calculation. Such calculations have been done in the context of charge transfer reactions before.[5,14,25,50] In Appendix A, we present a Landau−Zener derivation to span the nonadiabatic to adiabatic regimes that is well suited to our molecular dynamics simulation methodology. The dimensionless parameter of the LZ theory is

$$\bar{v}_0^{n_in_f} \equiv (v_0^{n_in_f}/v_T) = \frac{2\pi V^2_{n_in_f}}{\hbar\omega_s\sqrt{2\lambda_s k_B T}} \qquad (2.18)$$

Here, v_T is the thermal velocity,

$$v_T = \sqrt{k_B T/m_s} \qquad (2.19)$$

obtained by expressing the solvent Hamiltonian as an oscillator with coordinate x, velocity $v = \dot{x}$, and mass m_s and frequency ω_s. The solvent reorganization energy can be obtained from the relation $\lambda_s = (1/2)m_s\omega_s^2 d^2$, where the length d is the displacement of the final proton equilibrium position relative to the initial-state equilibrium position, due to solvent nuclear degrees of freedom. An approximate explicit form for each channel rate constant then is

$$k^{LZ}_{n_in_f} = \frac{\omega_s}{2\pi}\{[1 - e^{-\bar{v}_0^{n_in_f}}][1 - e^{-\bar{v}_0^{n_in_f}}/2]^{-1}\} \times G(\bar{v}_0^{n_in_f})e^{-(\lambda_s+\Delta G^0+E^f_{n_f}-E^i_{n_i})^2/(4\lambda_s k_B T)} \qquad (2.20)$$

where

$$G(\bar{v}_0^{n_in_f}) = \left[(1 - e^{-2\bar{v}_0^{n_in_f}}) + \frac{\sqrt{\pi}}{2}e^{-2\bar{v}_0^{n_in_f}}\right] \qquad (2.21)$$

There are two ingredients to this expression: The factor in the curly brackets { } is the (thermal) LZ probability of passage through a surface crossing accounting for multiple passages through the transition region.[5,51] In principle, this probability should be considered as a function of velocity and the rate constant evaluated as a velocity integral of the (one-way) flux through the crossing region. We have replaced this integral, as it is sharply peaked in velocity space, by an approximate form involving the thermal velocity as introduced in eq 2.19. The $G(\bar{v}_0^{n_in_f})$ factor then guarantees that the correct limiting forms, the nonadiabatic rate constant result, eq 2.16, and the adiabatic result,

$$k_{n_in_f} = \frac{\omega_s}{2\pi}e^{-(\lambda_s+\Delta G^0+E^f_{n_f}-E^f_{n_i})^2/(4\lambda_s k_B T)} \qquad (2.22)$$

are obtained when the LZ parameter in eq 2.18 is small and large, respectively. By numerical test, it is straightforward to show that the replacement of the velocity integral by the average velocity expression in eqs 2.20 and 2.21 is accurate to a few percent over the entire range of the LZ parameter. These channel rate constants $k_{n_in_f}$ are to be used in eq 2.16 to obtain the proton transfer rate constant.

$$k^{LZ} = \sum_{n_i}\rho_{n_i}\sum_{n_f}k^{LZ}_{n_in_f} \qquad (2.23)$$

The last quantity required for the evaluation of the LZ rate constant (it is not required for the nonadiabatic limit of eq 2.16) is the solvent frequency ω_s. This frequency may be obtained from the equipartition ratio of the fluctuations of v and x,[27] as follows from the oscillator Hamiltonian in eq A1:

$$\omega_s = \sqrt{\langle(\delta v)^2\rangle/\langle(\delta x)^2\rangle} \qquad (2.24)$$

where $\delta v = v - \langle v\rangle$ and $\delta x = x - \langle x\rangle$. The precise definition of the solvent coordinate, x, suitable to the polar−polarizable solvent model, is given at the end of section III.

III. Evaluation of Contributions to the Rate Constant

The formalism presented in section II requires the construction of various potential surfaces and wave functions and energies and matrix elements that are to be obtained from these surfaces. We now show how a combination of quantum mechanics and molecular dynamics may be used to obtain these ingredients to the rate constant.

For the gas-phase surface, we shall use a Lippincott Schroeder surface:[29,52]

$$V_g(r,R_{AB}) = be^{-aR_{AB}} + D_e[1 - e^{-n_A(r-d_A)^2/2r}] + CD_e[1 - e^{-n_B(R_{AB}-r-d_B)^2/2(R_{AB}-r)}] \qquad (3.1)$$

as it is a reasonable description of, for example, a NHO hydrogen-bonded system,[53] at least if some if its parameters are adjusted to fit *ab initio* data.[54] The parameters we use are $b = 2.4 \times 10^{13}$ kcal/mol, $a = 10.7$ Å^{-1}; $D_e = 110$ kcal/mol; $d_A = 0.95$ Å; $d_B = 0.97$ Å; $C = 0.85$; $n_A = 9.18$ Å, $n_B = 13.3$ Å. The "C" parameter is critical in establishing the stability of the complex in the gas phase: as chosen here, for all bonding distances of the R_{AB} coordinate, the stable configuration is the neutral one. However, this is not the surface that is relevant to this kind of proton transfer reaction, as we have discussed in section II.

To find the proton transfer surface, we must electronically solvate V_g. The solvent we use is dichloromethane. It is a polar−polarizable solvent that has a fairly large electronic polarizability, but does not have strong directional bonding tendencies; for example, it is not a hydrogen-bonding solvent.

TABLE 1: Interaction Parameters for the Solvent and Solute Molecules

site	mass	charge/|e|	α/Å^3	σ/Å[a]	ϵ/(kcal/mol)[a]
CH_2	14	0.340	0.338	3.96	0.1402
Cl	35	−0.170	2.810	3.35	0.3449
O[c]	93	−0.5 (−1.0)[b]		3.50	0.572
H		0.5 (0.5)[b]		0.00	0.000
N[c]	59	0.0 (0.5)[b]		3.50	0.572
CH_2−Cl = 1.772 Å			Cl−CH_2−Cl = 111.8°		dipole = 1.6 D
AHB = 2.7 Å[d]					

[a] σ and ϵ are the Lennard-Jones parameters. [b] Initial (final) proton state charges. [c] The masses are of the phenol and trimethylamine groups. [d] The approximate equilibrium value of R_{AB} (there is a slight variation with proton position).

We have previously devised a polar−polarizable molecular dynamics model for dichloromethane that does an adequate job of obtaining its structural and thermodynamic properties.[21] It is characterized by three sites with charges, q_i, site polarizabilities, α_i, and Lennard-Jones parameters given in Table 1. The solute is characterized as two Lennard-Jones spheres to represent the flanking groups to the hydrogen (cf. Table 1 for solute parameters). The charges assigned to the three sites model the dipole moment of the solute before and after the proton transfer, whereby the complex's dipole moment shifts from 2.5 to 10.5 D, indicating the predominately neutral to charge transfer character of the initial and final states.[1] We use a simple interpolation of charge form to represent the change in charge distribution of the complex between its initial and final states. Clearly, a more accurate representation of this functional dependence can only come from quantum chemical results, but the precise form certainly will not influence our conclusions, qualitatively. Standard combining rules are used to obtain the Lennard-Jones site−site interactions between the solute and solvent. One solute and 255 CH_2Cl_2 solvent molecules were placed in a cubic cell with length 30.08 Å, corresponding to a density of 0.0094 Å^{-3}. The classical equations of motion were integrated with the leap-frog algorithm[55] using a 3.0 fs time step. The temperature was maintained at 298.0 K by velocity scaling. Periodic boundary conditions with the minimum image convention were employed. The bond constraints were enforced using the SHAKE procedure.[56] The potential was smoothly cut off to zero at half the box length.

With this model for the solute and the solvent, the molecular dynamics method outlined above can be used to obtain the electronic solvation of the solute. First, for a given solvent−solute configuration (fixed r, R_{AB}, R^N) we solve eqs 2.4 and 2.5 for the induced dipoles of the solvent and obtain the polarization energy via eq 2.3 to obtain V_{els}. This, with the gas-phase surface of eq 3.1, provides a pels surface. Then, the forces, including those from the induced dipoles and from the Lennard-Jones and electrostatic contributions, are used to advance the solvent configuration, and, for this new R^N, the new V_{els} is obtained. As an example of the role of electronic solvation, Figure 2 displays an average over R^N of pels surfaces for a series of proton coordinate values for the heavy-atom separation R_{AB} = 2.7 Å (essentially the equilibrium separation for V_g). It is evident that electronic solvation has a profound effect on the proton surface, as the electronic solvation switches the predominant proton state from the neutral to the charge transfer one. Note that, as discussed in the Introduction, the electronic solvation should be roughly half of the full equilibrium solvation.

In order to evaluate the coupling $V_{pr}(R_{AB})$ responsible for the proton transfer, the scheme that leads to eq 2.9 must be implemented. First, MD runs with electronic solvation incorporated, as discussed in the previous paragraph, are carried out with the proton localized to its initial and final states. For a given R^N and R_{AB}, the energies V_i and V_f are compared and, if sufficiently close, we then construct the entire proton potential for this solvent configuration, as discussed in the previous paragraph, but here for the special solvent configurations R^{N*} where V_i and V_f are essentially degenerate. The resulting double-well potential is fit to the form of a quartic

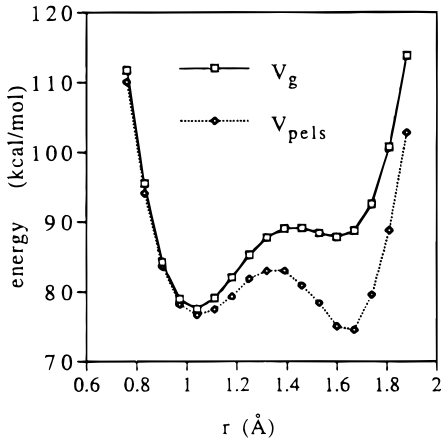

Figure 2. Proton gas-phase and pels (proton gas phase surface with electronic solvation) surfaces. The electronic solvation is equilibrated at each point along the proton coordinate. The left (right) well corresponds to the neutral (charge transfer) proton configuration. Electronic solvation can have a profound effect on the relative stability of these states by stabilizing the charge transfer state.

$$V_{pels}(r|R_{AB}) = \frac{\hbar\omega}{2}\left[-\frac{1}{2}\bar{r}^2 + \upsilon_4\bar{r}^4\right] \qquad (3.2)$$

with υ_4 a coefficient and ω the harmonic frequency of the proton (both υ_4 and ω depend on R_{AB}). In eq 3.2, we use units $\bar{r} = r/l$ scaled with the characteristic quantum length $l = \sqrt{\hbar/m\omega}$, where m is the proton mass. Solution of the Schrödinger equation of eq 2.8 with the potential surface of eq 3.2 provides the splitting whose configuration average $V_{pr}(R_{AB})$ is defined in eq 2.9. The solution is carried out with the use of a harmonic oscillator basis set and diagonalization of the resulting secular determinant.[57] The configuration dependent fluctuations of the splitting can be quite large, especially when the R_{AB} distance becomes short and the coupling becomes intrinsically large. The average behavior with R_{AB} is reasonably characterized by an exponential decay, as shown in Figure 3. A fit to the form

$$V_{pr}(R_{AB}) = V^o_{pr}(R_{AB})e^{-\alpha(R_{AB}-R^{eq}_{AB})} \qquad (3.3)$$

yields α = 35 Å^{-1} and V^o_{pr} = 0.045 kcal/mol, with R^{eq}_{AB} = 2.7 Å. An exponential dependence on R_{AB} is expected for values of R_{AB} that are sufficiently large to produce the requisite two-state system approximation, although at shorter distances this exponential distance dependence will go over to an approximately linear dependence.[14]

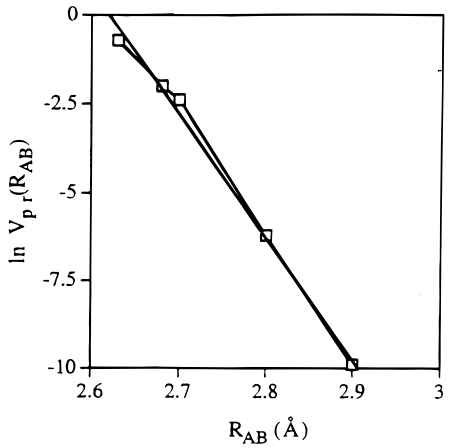

Figure 3. Logarithmic plot of the average protonic coupling matrix $V_{pr}(R_{AB})$ element as a function of the heavy-atom separation R_{AB}. The straight line is a fit to the data, showing that the coupling is reasonably exponential in this separation.

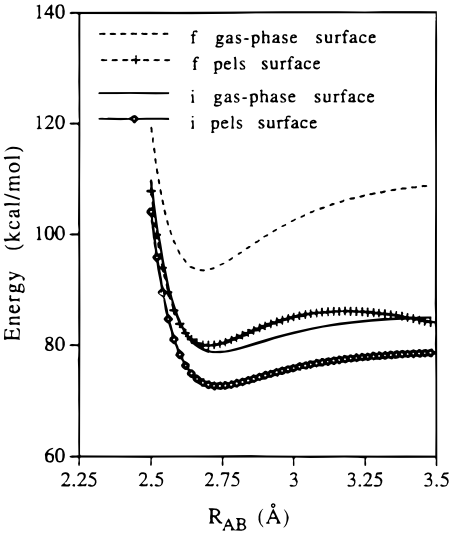

Figure 4. Gas-phase and pels surfaces dependence on R_{AB} for the proton initial (*i*) and final (*f*) states. Electronic solvation has a strong effect on the gas-phase surfaces; the *f*-state solvation is more dramatic than the *i*-state solvation as the *f* state corresponds to the charge transfer state and the *i* state to the neutral state.

Having found the proton coupling $V_{pr}(R_{AB})$, we now must evaluate its matrix elements $V_{n_i n_f}$ between the initial and final proton-localized states with wave functions $\phi^i_{n_i}(R_{AB})$ and $\phi^f_{n_f}(R_{AB})$, as defined in eq 2.17.

$$V_{n_i n_f} = \langle \phi^i_{n_i}(R_{AB}) | V_{pr}(R_{AB}) | \phi^f_{n_f}(R_{AB}) \rangle = \int dR_{AB}\, \phi^i_{n_i}(R_{AB})\, V_{pr}(R_{AB})\, \phi^f_{n_f}(R_{AB}) \quad (3.4)$$

To construct the pels surfaces from which we will obtain these wave functions (and corresponding energies), we now do MD simulations with the proton fixed at its initial or final state and, for a fixed R_{AB} distance, evaluate the induced dipoles again according to eqs 2.4 and 2.5 to obtain the electronic solvation energy from eq 2.3. Again, we configuration average this energy over a MD run that generates a sample of R^N values. This procedure is repeated for different R_{AB} values. In Figure 4, we present both the gas-phase and the pels surfaces, in order to see the effect that the electronic solvation has on their forms. It is evident that the electronic solvation is increasingly negative as R_{AB} increases and that this effect is more dramatic for the *f* (charge transfer) state. The shapes of the surfaces resemble Morse potentials, even when the electronic solvation is included, so we fit both surfaces to Morsians

$$V^i_{pels}(R_{AB}) = D^i_e[e^{-\kappa^i R_{AB}} - 1]^2 \quad (3.5)$$

with the parameters $\kappa^i = 5.11$ Å^{-1}, $D^i_e = 6.1$ kcal/mol and $\kappa^f = 5.7$ Å^{-1}, $D^f_e = 7.2$ kcal/mol. The *f* state surface deviates from a Morse form for large R_{AB}. However, as the matrix elements that are sufficiently large to contribute to the rate constant correspond to states relatively deep within the potential wells (*vide infra*), the deviation from the Morse form for large R_{AB} is not problematic. We then have the convenience of knowing the wave functions and energies from the standard Morse results. The origins of the two surfaces are displaced by $R^{i,eq}_{AB} - R^{f,eq}_{AB} = 0.037$ Å. The Morse surfaces support both bound and unbound states; the bound energy levels being given by the expression[58]

$$E^i_{n_i} = -D^i_e[1 - (\kappa^i l_i)^2 (n_i + 1)]^2 \quad (3.6)$$

where l_i is the quantum length for the reduced mass of the solute (~0.05 Å for both initial and final states). An analogous expression holds for the *f* state. The number of bound states n_M is found from the condition $1/(\kappa l)^2 > (n_M + 1/2)$ and is 12 for both the *i* and *f* pels surfaces. And, from the Morse energy expression, the deviation from harmonic behavior is already considerable for the n_i and $n_f = 3$ quantum numbers. Thus, these surfaces are quite anharmonic. (As we shall see, the rate constant will have contributions from about six quantum states, so this anharmonicity will be important to the rate constant's value.) The Morse eigenfunctions are given in terms of confluent hypergeometric functions and are available within Mathematica. Their normalized versions are also available.[59] With these eigenfunctions specified, and the protonic coupling $V_{pr}(R_{AB})$ known from eq 3.3, the matrix element in eq 3.4 can be evaluated by numerical integration.

The final ingredients required for the rate constant are the values of the solvent's frequency ω_s and contributions to the reorganization energy λ_s and the reaction free energy ΔG^0. We obtain these quantities by MD simulation, using an umbrella sampling method,[18,21,60−62] which provides good statistics around the, in principle, high-energy (relative to kT) crossing point of the solvent surfaces. Again, we account for the electronic polarization of the solvent with the use of our polar−polarizable solvent model.[21] In this fashion, the electronic polarization can be "extracted" so that the fluctuations responsible for driving the energetics to the correct configurations for the proton transfer correspond to the slow nuclear rearrangements. Thus, MD is run to obtain, for some R^N, the difference between the final and initial proton state's solute interaction with the solvent, allowing for the induced dipoles to be equilibrated to these charge distributions. This energetic difference serves as the reaction coordinate for the charge transfer and defines what we refer to as the coordinate x at the end of section II. For a MD run, the probability of finding different values of this energetic difference is constructed and the corresponding free energy surface's geometry serves to define the values of λ_s and ΔG^0. The umbrella sampling method accomplishes this by transferring the proton charge between initial and final states in sufficiently small steps so that, at any stage, the fluctuations of the solute−solvent interaction energy, away from the equilibrium value for the starting charge distribution, are not too much larger than thermal. The result of this simulation is a free energy surface that is, indeed, well represented as a parabola, from which the reorganization and reaction free energies can be extracted. Their values are $\lambda_s = 5.23$ kcal/mol and $\Delta G^0 = -7.3$ kcal/mol. If

TABLE 2: Thermally Weighted Squared Protonic Matrix Elements $\rho_{n_i}V_{n_in_f}^2$ (Normalized to Unity for the $n_i = n_f = 0$ Value) and Thermal Weights ρ_{n_i}: See Eq 4.1 and Following Discussion

	n_f									
n_i	0	1	2	3	4	5	6	7	8	ρ_{n_i}
0	1.0	0.46	0.17	0.064	0.025	0.011	0.0051	0.0025	0.0013	0.747 09
1	0.46	0.48	0.26	0.12	0.054	0.025	0.012	0.0064	0.0035	0.180 35
2	0.14	0.24	0.19	0.11	0.06	0.031	0.016	0.0087	0.0049	0.048 90
3	0.041	0.094	0.1	0.076	0.047	0.027	0.015	0.0086	0.005	0.014 90
4	0.012	0.033	0.045	0.041	0.029	0.019	0.012	0.007	0.0042	0.005 10
5	0.0035	0.012	0.019	0.02	0.016	0.012	0.0077	0.0049	0.0031	0.001 96
6	0.0011	0.0043	0.0078	0.0093	0.0085	0.0067	0.0047	0.0032	0.0021	0.000 85
7	0.0004	0.0017	0.0033	0.0044	0.0044	0.0037	0.0028	0.002	0.0014	0.000 41
8	0.00016	0.0007	0.0015	0.0021	0.0023	0.002	0.0016	0.0012	0.00084	0.000 22

these were the only contributions to the activation energy, the reaction would be quite close to activationless. The value of the solvent frequency ω_s can be obtained from the umbrella sampling runs by finite differencing the reaction coordinate x to obtain the velocity v and constructing a numerical approximation to ω_s as defined by eq 2.24. We have done this for each window in our umbrella sampling and find $\omega_s = 10 \pm 1$ ps^{-1}. In our evaluation of the rate constant, we shall use the average value $\omega_s \approx 10$ ps^{-1}.

IV. Results

The rate constant for proton transfer can now be evaluated with the use of eq 2.20 and 2.21, as all the factors that appear in them are available, as discussed in section III. It is of interest to examine the sizes of the different contributions to the rate expression. In particular, in Table 2, we display the thermally weighted protonic matrix elements

$$\rho_{n_i}|\langle\phi^i_{n_i}(R_{AB})|V_{pr}(R_{AB})|\phi^f_{n_f}(R_{AB})\rangle|^2 \tag{4.1}$$

as they are the most relevant for appreciating how many terms in the R_{AB} initial i and final f state Morse wells are required. The values in Table 2 have been normalized to the value of $\rho_{n_i=0}V_{n_i=0,n_f=0}$, for ease of comparison. We also list the thermal weights, ρ_{n_i}, of the i-state Morse well. A number of excited states in the initial and final R_{AB} wells contribute to the rate constant. The thermally weighted matrix elements do tend to be larger along the diagonal, but off-diagonal contributions are significant. Of course, these contributions are multiplied by the effective activation energies, and these can vary widely too.

A perspective on which distances R_{AB} are most significant in determining the value of the rate constant can be obtained by making the following assumptions: first, the diagonal elements of eq 4.1 are dominant; second, the displacement between the i and f Morse surfaces is small; and third, the Morse parameters of the two R_{AB} wells are not very different. In Appendix B, we show that, under these conditions, the rate constant in eq 2.16 can be approximated by

$$k_{diag} \approx [\int dR_{AB}\rho_i(R_{AB})V_{pr}{}^2(R_{AB})]\sqrt{\frac{\pi\hbar^2}{\lambda_s k_B T}}e^{-(\lambda_s+\Delta G^0)^2/(4\lambda_s k_B T)} \tag{4.2}$$

where $\rho_i(R_{AB})$ is the probability distribution of the Morse oscillator with the proton in its initial state. This average of the square of the protonic coupling then permits us to assess which distances R_{AB} are most important to the rate constant. For the problem at hand, the integrand of the R_{AB} integral in eq 4.2 is displayed in Figure 5 and shows that, as R_{AB} decreases from its equilibrium value by about 0.15 Å, the weight to the integral is cut off. Thus, as long as the two-level system approximation is valid for distances greater than this cut off,

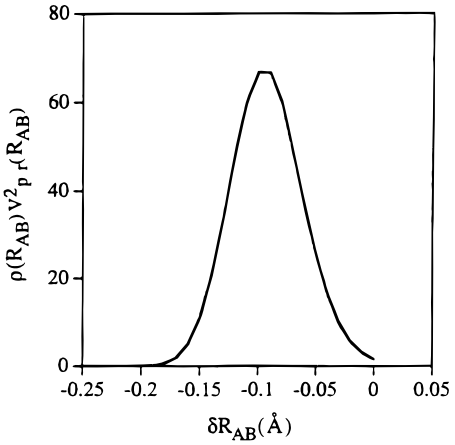

Figure 5. Dependence on heavy-atom separation $\delta R_{AB} = R_{AB} - R_{AB}^{eq}$ of the heavy-atom probability density $\rho(R_{AB})$ times the (squared) proton coupling matrix element $V_{pr}(R_{AB})$. (See eq 4.2.) The width of this function gives a qualitative picture of which distances contribute to the rate constant. Even though $V_{pr}(R_{AB})$ is exponentially increasing as R_{AB} decreases, the probability density provides a cutoff to control this increase.

the main contribution to the proton transfer rate constant will be from the mechanism discussed herein. This estimate is actually somewhat conservative, as it uses the nonadiabatic version of the rate expression. For the larger values of V_{pr}-(R_{AB}), where the reaction becomes adiabatic, the cut off at smaller values of R_{AB} will be more rapid than in Figure 5. Thus, the important values of R_{AB} are actually somewhat larger than those predicted by use of the nonadiabatic limit.

Evaluating the LZ rate constant given by eqs 2.20, 2.21, and 2.23, with all the factors accounted for, results in a rate constant of 1.42 ps^{-1}. (If we use the nonadiabatic expression of eq 2.16, the rate constant is 2.66 ps^{-1}.) Thus, the proton transfer rate constant is quite large. This fast rate can be traced to the following features. The pels surfaces for the i and f states of the proton are quite similar, and the displacement of their origins is small. So, the generalized Franck−Condon factors $V_{n_in_f}$ are relatively large. If there were a significant displacement between the origins of the i and f state wells, signaling a large reorganization energy in the R_{AB} coordinate, then these generalized Franck−Condon factors could be small. In the absence of the energetics arising from the R_{AB} coordinate, the energies $E^i_{n_i}$ and $E^f_{n_f}$, the solvent reorganization energy λ_s, and free energy ΔG^0 are quite close in value, and this makes the activation energy quite small. Note that the free energy ΔG^0 is the sum of the solvation free energy ΔG^{sol} and the contribution from the electronic structure of the solute. The LS surface indicates that the contribution from the electronic structure is 13.9 kcal/mol; the charge transfer state is endothermic, relative to the neutral state. Thus, the solvation free energy ΔG^{sol} is quite exothermic, about (−7 − 14) kcal/mol = −21 kcal/mol,

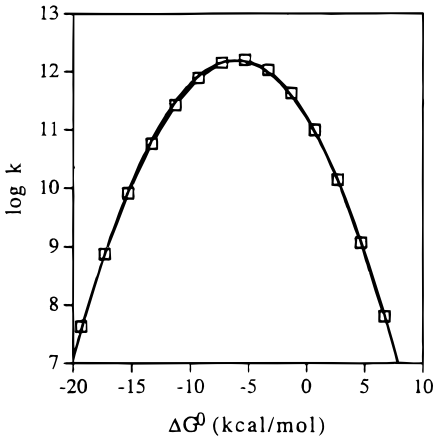

Figure 6. Logarithmic plot of the proton transfer rate constant versus driving force of the reaction. The data look parabolic, as would be obtained in a similar plot for a one classical (solvent) mode electron transfer rate expression. Here, however, the width of the parabola is not simply related to the solvent reorganization energy.

consonant with the charge transfer, large-dipole character of the final state, relative to the neutral, small-dipole initial state. Finally, the coupling $V_{pr}(R_{AB})$ responsible for the proton transfer is large for smaller values of R_{AB}; if these R_{AB}'s have significant weight, then the proton rate constant can be large.

Now, for the phenol−ammonia charge transfer complex, we have evaluated a ΔG^0 that includes the contributions from solvation and the electronic structure of the solute. When series of phenol−ammonia complexes are considered, the electronic structure contribution can vary significantly (eV scale), and the change can have a major effect on the rate constant. To investigate this effect, we simply change ΔG^0 in the expression for the rate constant and reevaluate it. A "Marcus" plot of this is shown in Figure 6. It is interesting to note that it looks not unlike typical Marcus plots in electron transfer studies that change the reaction free energy. But, the width of the plot is not simply related to the reorganization energy, as it would be for an electron transfer rate constant.

V. Concluding Remarks

The approach to proton transfer that we have pursued focuses on cases where the hydrogen bonding is relatively weak so that a double-well picture with a pair of well-localized tunnel states, which is the basis of a two-level system approach, can be identified. As we have noted, the correct surface with which to assess the validity of the two-level system approach is the electronically solvated surface. Electronic solvation does tend to deepen the proton potential surface, and this tends to reduce the proton coupling $V_{pr}(R_{AB})$, relative to its gas-phase value. Even with the electronic solvation effect, the R_{AB} dependence of $V_{pr}(R_{AB})$ is still very dramatic: we find a decay exponent of $\alpha \approx 35$ Å^{-1}. Since the solvent nuclear configurations relevant to calculating $V_{pr}(R_{AB})$ are the symmetrized ones, the electronic solvation just tends to deepen the double well, and, therefore, by WKB arguments, we still should expect to obtain an exponential dependence on R_{AB}.

The other key role of electronic solvation is to modify the R_{AB} surfaces for the initial and final proton states. Especially for the final, charge transfer state, the electronic solvation is quite strong, as shown in Figure 4. The displacement of charge with changing R_{AB} produces a substantial electronic solvation effect, as it does for the proton coordinate surface. The effect is to modify the wave functions $\phi^i_{n_i}(R_{AB})$ ($\phi^f_{n_i}(R_{AB})$) and energies $E^i_{n_i}$ ($E^f_{n_i}$) for the initial (final) states from their gas-phase values. The wave functions and energies in the pels surfaces $V^i_{pels}(R_{AB})$ and $V^f_{pels}(R_{AB})$ are explicit in the rate expression, because we treat the R_{AB} motion quantum mechanically. The R_{AB} frequency is sufficiently high ($\sim$250 cm^{-1}) to warrant a quantum treatment. Yet, it is not much greater than the thermal frequency; therefore, several states in these surfaces will contribute to the rate expression.

Another feature of the R_{AB} i and f surfaces is that they are not well represented as harmonic. The f-state electronic solvation's rapidly increasing magnitude with increasing R_{AB} pulls the pels surface $V^f_{pels}(R_{AB})$ away from the harmonic regime to make it even more Morse-like in character than the corresponding gas-phase surface. And, this naturally provides quantitatively different protonic matrix elements $V_{n_in_f}$ than would a harmonic approximation, as used in the analytic approaches.[10−13]

The rapid dependence of $V_{pr}(R_{AB})$ on R_{AB} makes the $V_{n_in_f}$ matrix elements completely different than the corresponding Franck−Condon factors (what the matrix element would be without $V_{pr}(R_{AB})$). Thus, the typical, strong dependence of the Franck−Condon factors on the relative displacement of the i and f surfaces' origins is not so important for the $V_{n_in_f}$. The origins of the pels surfaces, $V^i_{pels}(R_{AB})$ and $V^f_{pels}(R_{AB})$, that we have found are very close, indicating a small displacement of the surfaces upon proton transfer, and the shapes of the surfaces are not too different. If this feature is general, then there will be little reorganization from the R_{AB} mode, and the rate of decay of the protonic coupling $V_{pr}(R_{AB})$ will be pre-eminent in determining the rate.

The proton transfer mechanism featured in this work is restricted to a two-level system reduction. We stressed that, in a qualitative sense, the breakdown of this regime could be assessed by examining which R_{AB} distances are important to the proton transfer. Since the probability of finding a value of R_{AB} falls rapidly with decreasing R_{AB}, according to the density matrix $\rho_i(R_{AB})$, even though $V_{pr}(R_{AB})$ increases rapidly with decreasing R_{AB}, only R_{AB} values in a relatively small width around the most probable value for R_{AB} will contribute to the rate expression. Thus, the two-level system approximation will be valid, others things being equal, for higher values of the R_{AB} vibrational frequency.

Finally, we note that the proton transfer step can be viewed as the formation of a contact ion-pair. This ion-pair may dissociate to form, first, a solvent-separated ion-pair and may eventually dissociate to form solvated ions, A^- and HB^+. The transformation from the neutral species A--H−B to the solvated ions can then be viewed as a sequence of consecutive "reactions". The potential surfaces for these later steps will also be influenced, in part, by electronic solvation; consequently, the rates of these steps will depend on a proper accounting of this solvation. In the extreme, it is possible for the electronic solvation to so strongly solvate the surface for the first step, A--H−B → A^-−H--B^+, as to make it a dissociative surface. Then the overall process leading to solvated ions could be described as a one-step concerted reaction, and this would require a rather different perspective than is usually pursued for these reactions.

Acknowledgment. The financial support of the National Institutes of Health (GM 47274) is gratefully acknowledged.

Appendix A

In this Appendix, we derive the Landau−Zener version of the proton transfer rate constant presented in eqs 2.20 and 2.21. We may define the rate constant from a flux formula. It is evident that since the rate constant k is a sum over channel rates,

we may do the derivation for a specific channel rate constant $k_{n_i n_f}$ and add the results with the initial-state weighting as in eq 2.16. To not burden the notation, we will not indicate which surface crossing we are treating, until the end. A flux expression for the rate constant is[5,50]

$$k = \int_0^\infty d\upsilon \int dx\, f^{eq}(x,\upsilon)\, \upsilon P(\upsilon)\, \delta(x - x^*) / \int_{-\infty}^{\infty} d\upsilon \int dx\, f^{eq}(x,\upsilon) \tag{A.1}$$

Here, x and υ are defined via the displaced oscillator Hamiltonians:[3]

$$H_i = \frac{1}{2} m_s \upsilon^2 + \frac{1}{2} k_s x^2$$

$$H_f = \frac{1}{2} m_s \upsilon^2 + \frac{1}{2} k_s (x - d)^2 + \Delta G^0 \tag{A.2}$$

The length d is the displacement of the final state, relative to the initial state, and $\upsilon = \dot{x}$ is the conjugate velocity. The force constant k_s and mass m_s are related by $k_s = m_s \omega_s^2$, which serves as a definition of the solvent frequency ω_s, and the solvent reorganization energy λ_s is defined as $\lambda_s = (1/2) m_s \omega_s^2 d^2$. The value of x^* in the delta function is the energy of the crossing point for the particular channel indexed by the quantum numbers n_i and n_f. It leads to the effective activation energies as given in eq 2.16. (The coordinate x corresponds in the molecular dynamics simulation to the energy difference between the solute−solvent interaction for a fixed solvent nuclear configuration R^N with the electronic polarization in equilibrium with the respective charge distributions of the initial and final states.)

The equilibrium (unnormalized) distribution function is

$$f^{eq}(x,\upsilon) = f^{eq}(x)\, f^{eq}(\upsilon) = e^{-V_i(x)/k_B T} e^{-m_s \upsilon^2 / 2 k_B T} \tag{A.3}$$

$P(\upsilon)$ is the transition probability allowing for multiple crossings of the surface intersection point:[51]

$$P(\upsilon) = [1 - e^{-\upsilon_0/\upsilon}][1 - e^{-\upsilon_0/\upsilon}/2]^{-1} \tag{A.4}$$

It is used for positive velocities, as the integral in eq A.1 indicates. The Landau−Zener parameter υ_0 is given by[48,49]

$$\upsilon_0 = \frac{2\pi V^2}{|\hbar \partial (V_f - V_i)/\partial x|_{x=x^*}} = \frac{\pi V^2}{\hbar k_s d} \tag{A.5}$$

The second equality in eq A.5 follows from eq A.2. The expression in eq A.1 could be used to evaluate the channel rate constants. However, as it is evident that the integrand of eq A.1 is peaked around the thermal velocity,

$$\upsilon_T = \sqrt{k_B T / m_s} \tag{A.6}$$

the integral can be approximated in terms of the integrand evaluated around the thermal velocity. There are several ways to do this. As we know that the nonadiabatic limit of the rate constant must follow for $\bar{\upsilon}_0 = \upsilon_0/\upsilon_T \to 0$, while the adiabatic limit, where the prefactor of the rate constant should be $\omega_s/2\pi$,[17] must follow for $\bar{\upsilon}_0 \to \infty$, we may introduce a simple interpolating factor to produce these limits. And we may then check the interpolation formula by comparison with the value obtained from the velocity integration of eq A.1. In this fashion we find that

$$\langle F \rangle_v = \int_0^\infty d\upsilon \upsilon\, P(\upsilon)\, f^{eq}(\upsilon) / \int_{-\infty}^{\infty} d\upsilon\, f^{eq}(\upsilon) \approx F(\bar{\upsilon}_0)\, G(\bar{\upsilon}_0) \tag{A.7}$$

where

$$G(\bar{\upsilon}_0) = \left[(1 - e^{-c\bar{\upsilon}_0}) + \frac{\sqrt{\pi}}{2} e^{-c\bar{\upsilon}_0} \right] \tag{A.8}$$

with $c = 4$ does interpolate accurately between the nonadiabatic and adiabatic limits.

To apply this expression to the proton transfer rate constant requires its use for all the crossings, described by the pairs n_i, n_f. The energies of the states in the R_{AB} Morse wells, $E^i_{n_i}$ and $E^f_{n_f}$, must be added to the solvation energies of eq A.2 in order to generate the force differences in the definition of υ_0, cf. eq A.5. Even though the energy levels $E^i_{n_i}$ ($n_i = 1,2, ...$) and $E^f_{n_f}$ ($n_f = 1,2, ...$) are not equally spaced, this does not affect the values of the forces, as

$$|\Delta F|_{n_i n_f} = |\partial (V_f + E^f_{n_f} - V_i - E^i_{n_i})/\partial x| = |\partial (V_f - V_i)/\partial x| = |\Delta F| = k_s d \tag{A.9}$$

The dependence on the quantum numbers n_i and n_f in eq A.5 then just resides in the matrix elements $V_{n_i n_f}$. That is why, in eq 2.18, the reorganization energy does not depend on the n_i and n_f indices. Combination of eqs A.5−A.8 then yields eq 2.18.

Appendix B

Here, we approximate the nonadiabatic rate constant expression of eq 2.16 by assuming that (1) only the diagonal elements of the $V_{n_i n_f}$ matrix contribute to the rate constant and (2) the Morse wells are similar in shape and are not displaced, relative to each other, by a significant amount. The Morse parameters given after eq 3.5, and the small ~0.04 Å displacement of the origins show that this is a reasonable approximation for our study. This means that the reorganization energy arising from the R_{AB} mode is negligible. Then, eq 2.16 becomes

$$k_{NA}^{diag} = \sum_{n_i} \rho_{n_i} V_{n_i n_i}{}^2 \sqrt{\frac{\pi \hbar^2}{\lambda_s k_B T}} e^{-(\lambda_s + \Delta G^0 + E^f_{n_i} - E^i_{n_i})^2/(4\lambda_s k_B T)} \approx \sum_{n_i} \rho_{n_i} V_{n_i n_i}{}^2 \sqrt{\frac{\pi \hbar^2}{\lambda_s k_B T}} e^{-(\lambda_s + \Delta G^0)^2/(4\lambda_s k_B T)} \tag{B.1}$$

The approximate equality in eq B.1 relies on neglecting the difference in energies that are supported by the initial and final state R_{AB} wells; $E^i_{n_i} \approx E^f_{n_i}$, as consistent with assuming the Morse parameters for the i and f state wells are essentially the same. The thermally weighted matrix element can be rewritten as

$$\sum_{n_i} \rho_{n_i} V_{n_i n_i}{}^2 = \sum_{n_i} \rho_{n_i} |\langle \phi^i_{n_i}(R_{AB}) | V_{pr}(R_{AB}) | \phi^i_{n_i}(R_{AB}) \rangle|^2$$

$$= \int dR_{AB} V_{pr}{}^2(R_{AB}) \sum_{n_i} \rho_{n_i} [\phi^i_{n_i}(R_{AB})]^2$$

$$= \int dR_{AB} V_{pr}{}^2(R_{AB}) \rho_i(R_{AB}) \tag{B.2}$$

The last equality employs the definition of the position representation of the initial state density matrix, $\rho_i(R_{AB})$. Combining eqs B.1 and B.2 yields eq 4.2. If we use a harmonic oscillator instead of the Morse potential for the R_{AB} wells, then

the integral over R_{AB} in the last integral of eq B.2 is readily carried out to yield

$$\int dR_{AB} V_{pr}^{\,2}(R_{AB})\, \rho_i(R_{AB}) = e^{2\alpha^2\langle (R_{AB}-R_{AB}^{eq})^2\rangle} = e^{2\alpha^2(\hbar/2m\omega)\coth(\hbar\omega/kT)} \quad \text{(B.3)}$$

When combined with eq B.1, this yields a known approximate formula for the proton transfer rate constant.[10−13]

References and Notes

(1) Zeeger-Huyskens, T.; Huyskens, P. In *Molecular Interactions*; Ratajczak, H., Orville-Thomas, W. J., Eds.; Wiley: New York, 1980; Vol. 2; p 1.
(2) Zhu, J. J.; Cukier, R. I. *J. Chem. Phys.* **1995**, *102*, 8398.
(3) *Physical Chemistry−An Advanced Treatise*; Levich, V. G., Ed.; Academic: New York, 1970; Vol. 9B, p 985.
(4) Marcus, R. A.; Sutin, N. *Biochim. Biophys. Acta* **1985**, *811*, 265.
(5) Ulstrup, J. *Charge Transfer Processes in Condensed Media*; Springer: Berlin, 1979.
(6) Scheiner, S. In *Proton Transfer in Hydrogen-Bonded Systems*; Bountis, T., Ed.; Plenum: New York, 1992; Vol. 291, p 29.
(7) Scheiner, S.; Duan, X. In *Modelling the Hydrogen Bond*; Smith, D. A., Ed.; ACS Symposium Series: Washington, DC, 1994; Vol. 569, p 125.
(8) Benderskii, V. A.; Goldanski, V. I.; Ovchinnikov, A. A. *Chem. Phys. Lett.* **1980**, *73*, 492.
(9) Benderskii, V. A.; Goldanski, V. I.; Makarov, D. E. *Phys. Rep.* **1993**, *233*, 195.
(10) Borgis, D.; Lee, S.; Hynes, J. T. *Chem. Phys. Lett.* **1989**, *162*, 19.
(11) Morillo, M.; Cukier, R. I. *J. Chem. Phys.* **1990**, *92*, 4833.
(12) Suárez, A.; Silbey, R. *J. Chem. Phys.* **1991**, *94*, 4809.
(13) Borgis, D.; Hynes, J. T. *Chem. Phys.* **1993**, *170*, 315.
(14) Borgis, D.; Hynes, J. T. *J. Phys. Chem.* **1996**, *100*, 1118.
(15) Marcus, R. A. *J. Chem. Phys.* **1956**, *24*, 966.
(16) Marcus, R. A. *J. Chem. Phys.* **1965**, *43*, 679.
(17) Marcus, R. A. *Annu. Rev. Phys. Chem.* **1964**, *15*, 155.
(18) King, G.; Warshel, A. *J. Chem. Phys.* **1990**, *93*, 8682.
(19) Warshel, A.; Levitt, M. *J. Mol. Biol.* **1976**, *103*, 227.
(20) Enomoto, Y.; Kakitani, T.; Yoshimori, A. *Chem. Phys. Lett.* **1991**, *186*, 366.
(21) Zhao, X. G.; Cukier, R. I. *J. Phys. Chem.* **1995**, *99*, 945.
(22) Vesely, F. *J. Comput. Phys.* **1977**, *24*, 361.
(23) Ahlström, P.; Wallqvist, A.; Engström, S.; Jönsson, B. *Mol. Phys.* **1989**, *69*, 563.
(24) Cukier, R. I.; Karkheck, J.; Kumar, S.; Sheu, S. Y. *Phys. Rev. B* **1990**, *41*, 1630.
(25) Warshel, A. *J. Phys. Chem.* **1982**, *86*, 2218.
(26) Borgis, D.; Hynes, J. T. *J. Chem. Phys.* **1991**, *94*, 3619.
(27) Staib, A.; Borgis, D.; Hynes, J. T. *J. Chem. Phys.* **1995**, *102*, 2487.
(28) Borgis, D.; Tarjus, G.; Azzouz, H. H. *J. Phys. Chem.* **1992**, *96*, 3188.
(29) Azzouz, H.; Borgis, D. *J. Chem. Phys.* **1993**, *98*, 7361.
(30) Truong, T. N.; McCammon, J. A.; Kouri, D. J.; Hoffman, D. K. *J. Chem. Phys.* **1992**, *96*, 8136.
(31) Bala, P.; Lesyng, B.; McCammon, J. A. *Chem. Phys.* **1994**, *180*, 271.
(32) Hammes-Schiffer, S.; Tully, J. C. *J. Chem. Phys.* **1994**, *101*, 4657.
(33) Hammes-Schiffer, S.; Tully, J. C. *J. Phys. Chem.* **1995**, *99*, 5793.
(34) Laria, D.; Ciccotti, G.; Ferrario, M.; Kapral, R. *J. Chem. Phys.* **1992**, *97*, 378.
(35) Consta, S.; Kapral, R. *J. Chem. Phys.* **1994**, *101*, 10908.
(36) Mavri, J.; Berendsen, H. J. C.; Gunsteren, W. F. v. *J. Phys. Chem.* **1993**, *97*, 13469.
(37) Berendsen, H. J. C.; Mavri, J. *J. Phys. Chem.* **1993**, *97*, 13464.
(38) Mavri, J.; Berendsen, H. J. C. *J. Phys. Chem.* **1995**, *99*, 12711.
(39) VanDerSpoel, D.; Berendsen, H. J. C. *J. Phys. Chem.* **1996**, *100*, 2535.
(40) Li, D. H.; Voth, G. A. *J. Phys. Chem.* **1991**, *95*, 10425.
(41) Lobaugh, J.; Voth, G. A. *Chem. Phys. Lett.* **1992**, *198*, 311.
(42) Lobaugh, J.; Voth, G. A. *J. Chem. Phys.* **1994**, *100*, 3039.
(43) Marcus, R. A. *J. Chem. Phys.* **1956**, *24*, 979.
(44) Böttcher, C. J. F. *Theory of Electrical Polarization*, 2nd ed.; Elsevier: Amsterdam, 1973; Vol. I.
(45) DeVault, D. *Quantum Mechanical Tunneling in Biological Systems*; Cambridge University Press: London, 1984.
(46) Kestner, N. R.; Jortner, J.; Logan, J. *J. Phys. Chem.* **1974**, *78*, 2148.
(47) Cukier, R. I. *J. Phys. Chem.* **1995**, *99*, 16101.
(48) Landau, L. D. *Phys. A. Sowjetunion* **1932**, *2*, 46.
(49) Zener, C. *Proc. R. Soc. London Ser. A* **1932**, *37*, 696.
(50) Cukier, R. I.; Nocera, D. G. *J. Chem. Phys.* **1992**, *97*, 7371.
(51) Nikitin, E. E.; Umanskii, S. Y. *Theory of Slow Atomic Collisions*; Springer-Verlag: Berlin, 1984.
(52) Lippincott, E. R.; Schroeder, R. *J. Chem. Phys.* **1955**, *23*, 1099.
(53) Gilli, P.; Bertolasi, V.; Ferretti, V.; Gilli, G. *J. Am. Chem. Soc.* **1994**, *116*, 909.
(54) Vener, M. V. *Chem. Phys. Lett.* **1995**, *244*, 89.
(55) Allen, M. P.; Tildesley, D. *Computer Simulation of Liquids*; Clarendon: Oxford, 1987.
(56) Ryckaert, J. P.; Ciccotti, C.; Berendsen, J. J. C. *J. Comput. Chem.* **1977**, *23*, 327.
(57) Somorjai, R. L.; Hornig, D. F. *J. Chem. Phys.* **1962**, *36*, 1980.
(58) Landau, L. D.; Lifshitz, E. M. *Quantum Mechanics*; Pergamon Press: Oxford, 1965; Vol. 3.
(59) Feagin, J. M. *Quantum Methods with Mathematica*; Springer-Verlag: New York, 1994.
(60) Huang, J.-K.; Warshel, A. *J. Am. Chem. Soc.* **1987**, *109*, 705.
(61) Kuharski, R. A.; Bader, J. S.; Chandler, D.; Sprik, M.; Klein, M. L.; Impey, R. W. *J. Chem. Phys.* **1988**, *89*, 3248.
(62) Chandler, D.; Kuharski, R. A. *Faraday Discuss. Chem. Soc.* **1988**, *85*, 329.